

# Determination of the optimal inversion parameters in recovering the 2015 Illapel Chile Tsunami source by the $r$ -solution method

T.A. Voronina

**Abstract.** This paper highlights the influence of the model parametrization, including the sea level recorders localization and source discretization, on the tsunami source inversion. Modeling the initial water displacement in the tsunami source area is based on the least square inversion and a truncated singular value decomposition approach that makes possible to overcome the instability of a numerical solution and to obtain an acceptable result in spite of the ill-posedness of the problem. This paper discusses the importance of the consideration of the parameter  $r$  in conjunction with the source spatial discretization. The results obtained allow one to explain the appearance of the artifacts in the solution by the truncation effect. Moreover, the optimal choice of such parameters as the spatial discretization of a source, the arrangement of the sea level recorders and the parameter  $r$  leads to a profound improvement in recovering the initial tsunami waveform. The methodology proposed has been verified by the numerical simulation of the 16 September 2015 Chile tsunami source.

## 1. Introduction

During the past fifteen years, many devastating tsunamis occurred in the Pacific and the Indian oceans. The problem of the tsunami timely warning is of great importance. False alarms are expensive and embarrassing. There are two important aspects of assessing the tsunami hazard in the coastal areas: the initial waves generated in the source area and their subsequent propagation. This study deals with the first of the above challenges.

Although a considerable attention has been given to developing the inversion mathematical methods to infer the initial tsunami waveform [1–10], but a lesser number of studies has been devoted to revealing the influence of such characteristics of observation systems as the number and the spatial distribution of the recording devices.

In order to correlate these notions, the approach to reconstruct an initial tsunami waveform based on the inversion of the remote measurements of water-level data was proposed by Voronina and Tcheverda in [11] and was already described in its fundamentals in previous papers [12–14].

In the present study, the problem of recovering a tsunami source from available measurements of an incoming wave is considered as an inverse

problem of mathematical physics. This inverse problem is treated as an ill-posed one and is regularized by means of the least square inversion using the truncated singular value decomposition (SVD) approach. To avoid the potential instability of the numerical solution, the  $r$ -solution method is used. The unknown function of a water surface displacement in the source area is approximated with the basis of the right singular vectors, which is the most adequate for the solution of ill-posed problems and is independent of the special function that allows one to distinguish the main stable part of the solution. In other words, the  $r$ -solution is a projection of the exact solution on a stable subspace which is linear hull of  $r$  first right singular vectors. This subspace is chosen by analyzing the properties of the singular spectrum of the direct problem operator, which, in turn, is determined by arranging the tsunami waveform recorders and bathymetry.

As was shown in a previous studies, a distinguishing feature of the method in question is a possibility to estimate the capability of a certain observational system to recover a tsunami source and to determine the most informative set of the sea level recorders.

This study focuses on the effect of truncating the space of the solution on the recovery of the spacial harmonics used in the representation of the source function. The number of harmonics used essentially affects on the time of calculation. Moreover, the effect revealed allows one to explain the appearance of some artifacts in the tsunami source form obtained.

## 2. The method

The inverse problem is in reconstructing the initial free surface elevation  $\vec{\eta}(x, y, t)|_{t=0}$  described by some finite function  $\varphi(x, y)$  with a support in the domain  $\Omega$  as output data, while input data are represented by the vector-function  $\vec{\eta}_0(t)$ :

$$\vec{\eta}_0(t) = (\eta(x_1, y_1, t), \dots, \eta(x_P, y_P, t))^T$$

with components of the marigrams  $\eta(x_p, y_p, t)$  known at a finite number of points (recorders)  $(x_p, y_p)$ ,  $p = 1, \dots, P$ .

The tsunami wave propagation is considered within the scope of the linear shallow-water theory. The curvature of the Earth is neglected. Suppose that the tsunami wave excitation is caused by an abrupt rising and sinking of the bottom at the initial time from a state of rest, and that the water surface is similar to the bottom shape in the tsunami source area. In the present paper, the processes of wave run-up on the shore structures are not considered. A source area, an  $l_1 \times l_2$  rectangle  $\Omega$ , is assumed to be known from seismic data. The coastline is assumed to be an absolutely reflecting rigid wall. The absolutely absorbing boundary conditions are applied on the so-called open boundaries.

This statement of the problem was already described in [14, 15]. The observed waveforms  $\vec{\eta}_0$  can be expressed as follows

$$\vec{\eta}_0(t) = A\varphi, \quad (1)$$

where the operator  $A$  is a compact linear operator of the first kind. This operator transforms the initial water elevation  $\varphi(x, y)$  to the data  $\vec{\eta}_0(t)$ . The properties of this operator have been investigated in [12, 16, 17]. As a compact operator  $A$  could be described in the Hilbert spaces with the singular system  $\{s_j, \vec{u}_j, \vec{v}_j\}$ ,  $j = 1, \dots, \infty$ , where  $s_j$  ( $s_1 \geq s_2 \geq s_3 \dots$ ) are singular values,  $\vec{u}_j$ ,  $\vec{v}_j$  are the left and the right singular vectors, and  $s_j \rightarrow 0$  at  $j \rightarrow \infty$ . The systems  $\{\vec{u}_j\}$ ,  $\{\vec{v}_j\}$  are orthogonal. A very important property of the singular vectors is that they form bases in the space of data and in the space of model, respectively. Also, the relation  $A\vec{v}_j = s_j\vec{u}_j$  is satisfied. Equation (1) can be reduced to an infinite system of linear algebraic equations. To solve this system numerically, a finite-dimensional approximation is used. The compactness of the operator under consideration means that as the dimensions of the subspaces induced by the finite-dimensional approximation increase, the sensitivity of the solution to errors also increases.

This obstacle can be avoided by restricting the operator to a subspace that is a linear hull of its first right singular vectors, and in this way, the so-called  $r$ -solution could be constructed [16].

For the numerical simulation, the unknown function of the water surface displacement  $\varphi(x, y)$  in the source area (the rectangle  $\Omega$ ) can be represented as a series of spatial harmonics  $\varphi_{mn}(x, y) = \sin \frac{m\pi}{l_1}x \cdot \sin \frac{n\pi}{l_2}y$ :

$$\varphi(x, y) = \sum_{m=1}^M \sum_{n=1}^N c_{mn} \varphi_{mn}(x, y)$$

with the vector of unknown coefficients  $\vec{c} = \{c_{mn}\}$ . The vector  $\vec{\eta}$  containing the discrete observed waveforms

$$\vec{\eta} = (\eta_{11}, \dots, \eta_{1N_t}, \dots, \eta_{P1}, \dots, \eta_{PN_t})^T$$

in the components (marigrams)  $\eta_{pj} = \eta(x_p, y_p, t_j)$  at a set of points  $(x_p, y_p)$ ,  $p = 1, \dots, P$ , and for the time instants  $t_j$ ,  $j = 1, \dots, N_t$ , is expressed as superposition of the computed waveforms as follows

$$\vec{\eta} = A\vec{c}, \quad (2)$$

where  $A$  is a matrix whose columns are the computed synthetic waveforms based on the shallow-water theory with every spatial harmonic used as a source. Thus, the dimension of the space of solutions for the discrete problem is  $M \times N$ , and the total dimension of the space of discrete input data is

$P \times N_t$ . The matrix  $A$  admits the singular value decomposition  $A = U\Sigma V^T$ , where  $U$  and  $V$  are the orthogonal matrices whose columns are the left ( $\vec{u}_j$ ) and the right ( $\vec{v}_j$ ) singular vectors of the matrix  $A$ , respectively. The matrix  $\Sigma$  is a diagonal one with the singular values  $s_j$  of the matrix  $A$  on the main diagonal. As a result of the numerical process, the so-called  $r$ -solution of equation (2)  $\vec{c}^{[r]} = \sum_{j=1}^r \alpha_j \vec{v}_j$  is obtained. Finally, the  $r$ -solution of equation (1) is obtained in the form

$$\varphi^{[r]}(x, y) = \sum_{j=1}^r \alpha_j \sum_{m=1}^M \sum_{n=1}^N \beta_{mn}^j \varphi_{mn}(x, y),$$

where  $\alpha_j = \frac{(\vec{\eta}, \vec{u}_j)}{s_j}$  and  $\vec{v}_j = (\beta_{11}^j, \dots, \beta_{MN}^j)^T$ . Setting the parameter  $d$ , one can determine a possible value  $r$  by the relation  $r = \max\{k : s_k/s_1 \geq d\}$ .

The number  $r$  is taken to be much smaller than a minimum dimension of the matrix. It is natural that as  $r$  increases, the amount of information on the  $r$ -solution obtained also increases, while the stability decreases.

The location of tsunami waveforms recorders affects the choice of the value  $r$  by such a way: the better is the configuration of the observation system the longer is a weakly decreasing part of the spectrum. It is clear that the behavior of the singular spectrum is determined by the observational system and bathymetry. We cannot change the bathymetry but can influence the design of the observational system. Analyzing the singular spectra of the matrices obtained one can estimate the quality of the inversion to be done by a certain observational system and propose a more effective disposition for the tsunami wave recorders.

### 3. Application to the Chile Tsunami case

The 2015 Illapel earthquake occurred at 22:54:32 (UT) on 16 September, at 31.573°S, 72.674°W at 22.4 km depth (according to the United States Geological Survey). This earthquake as well as the associated tsunami have been studied by many researchers from various aspects allowing them to design slightly different models of the earthquake source based on the various geophysical data: near-field seismograms, teleseismic waveform and back projections, GPS and InSAR data, and tsunami waveforms [18]. There has also been determined a tsunami source area, approximately, 70 km to the NW of the epicenter by the method of the backward ray tracing of the observed tsunamis [19]. The distribution of tsunami heights was assumed to be consistent with the slip distribution, their maxima vary from 4 to 12 m.

In this study, the inversion method described above was applied to the 2015 Illapel event to recover the tsunami source by the inversion of the tsunami waveforms recorded only by the Deep-ocean Assessment and Reporting of Tsunamis (DART).

The simulation domain is the water part of the rectangle  $\Pi = \{(x, y) : 102^\circ\text{W} \leq x \leq 70^\circ\text{W}; 12^\circ\text{N} \leq y \leq 38^\circ\text{S}\}$ . It is covered by a 1-minute grid of  $1921 \times 3001$  points to follow GEBCO bathymetry (<http://www.gebco.net/>). The source area is assumed to be  $\Omega = \{71.6^\circ\text{W} \leq x \leq 73^\circ\text{W}; 30^\circ\text{S} \leq y \leq 32.5^\circ\text{S}\}$ . It is covered by a grid of  $77 \times 151$  points. The DART data are provided by the National Oceanic and Atmospheric Administration (NOAA) of the United States (<http://www.ndbc.noaa.gov/dart.shtml>). At the coastal boundaries of the calculation domain, conditions of full reflection, as well as at the open sea boundaries, the wave permeable conditions are formulated. The time step  $\Delta t = 4$  s, and the length of each marigram part being used  $N_t = 1001$ , beginning with the first arrival of the wave at the corresponding recorder. Figure 1 shows the calculation domain, source area and the observational system consisting of five deep-water recorders DART buoys numbered counterclock-wise and marked by magenta circles: 1—32402; 2—32401; 3—32412; 4—32411; 5—43413.

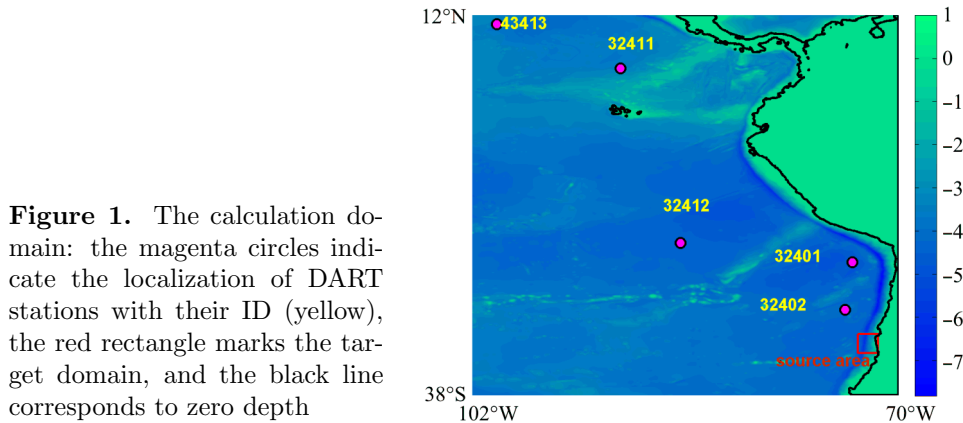


**Figure 1.** The calculation domain: the magenta circles indicate the localization of DART stations with their ID (yellow), the red rectangle marks the target domain, and the black line corresponds to zero depth

The original FORTRAN code is used to numerically simulate the tsunami propagation. It is based on a finite difference algorithm using an explicit-implicit difference scheme constructed with a four-point stencil on a uniform rectangular staggered grid [20]. The scheme is of second order of approximation with respect to space and of first order with respect to time.

Since the SVD truncation of the matrix  $A$  is the key component of the method proposed, one needs to know how it affects the solution of system (2). The decomposition of the right singular vectors with the basis of the spatial harmonics can be represented in the form

$$\vec{v}_j = \sum_{m=1}^M \sum_{n=1}^N \beta_{mn}^j \varphi_{mn}(x, y).$$

Figure 2 shows 64 right singular vectors decomposed to the spatial harmonics: the coefficients  $\beta_{mn}^j$  are represented on the axis  $Oz$ ; the harmonics

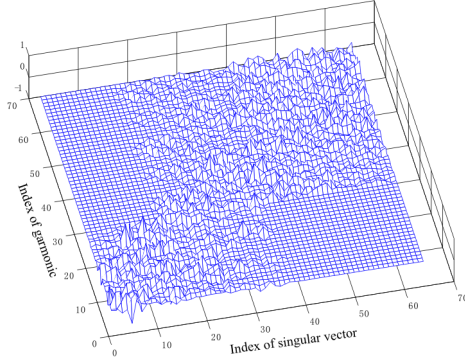


**Figure 2**

high-frequency sea surface oscillations. On the contrary, when one uses a small number of the first singular vectors to represent the solution, the high-frequency harmonics are poorly represented for this set of singular vectors, and as a result, one obtains a fairly “rude” form of the source with the low extreme values. The behavior of the right singular vectors presented in Figure 2 with respect to the spatial harmonics remains structurally the same even if the dimension of the full space changes. The structure of the right singular vectors is predetermined by the location of the observation system and the bottom relief in the simulation domain.

How many spatial harmonics are reasonable? The value of the angle between the vector of each harmonic  $\varphi_k$  and the subspace of a quasi-solution will determine the contribution of each harmonic to the solution obtained. The cosines of the angles between the subspace corresponding to  $r = 37$  and the spatial harmonics  $\varphi_k$ ,  $k = 1, \dots, 225$  ( $M = N = 15$ ) were computed and are shown in Figure 3—there are the indices of the harmonics in  $x$

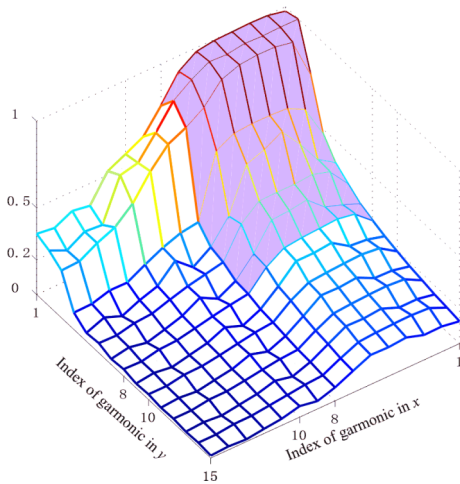


**Figure 3**

$\{\varphi_k\} = \{\varphi_{mn}\}$  are enumerated in the order:  $k = n + (m - 1) \times N$ ,  $m = 1, \dots, M$  (in longitude),  $n = 1, \dots, N$  (in latitude).

It is clear from Figure 2 that 40 first right singular vectors contain the components corresponding to both the low- and the high-frequency harmonics. Using the singular vectors with large indices will result in the “dispersion” of the form of the source into numerous

(in longitude) and in  $y$  (in latitude) on the horizontal axes and the vertical axis corresponds to the cosine values. It is clear from Figure 3 that the harmonics with the indices exceeding 8 in the latitude and the longitude have bigger angles. Moreover, one can note a sharp decrease of the cosine values when their indices exceed 8. The smaller cosine values mean that the corresponding harmonics are poorly represented within the truncated subspace and, thus, their contribution to the  $r$ -solution will be small, whereas numerical artifacts would be large.

In the numerical experiments, the following fact was found out: each harmonic is only precisely reconstructed (99.8%) on the space based on a full set of the right singular vectors (for the case of noiseless data). Moreover, when a truncated subspaces are used for the reconstruction, a series of additional harmonics (mostly, high-frequency) appear including a noticeable distortion of the amplitude. A decrease of the parameter  $r$  has a greater effect on the higher-frequency harmonics. The higher is frequency, the larger are artifacts. These facts contribute to the understanding that artifacts in the solution are inevitable and are caused by the ill-posedness of the problem.

Hence, one can conclude that for the case under consideration the optimal number of the spatial harmonics varies from 49 to 64 ( $M = 7, 8$ ;  $N = 7, 8$ ).

The results of the tsunami source recovery for the Illapel Chile Tsunami based on the optimal parameters revealed in the course of the discussion above are represented in Figure 4 with the following designation: the black line indicates to the inferred tsunami source area according to [19], the yellow line indicates to the axis of the trench, and the red circle indicates to the earthquake epicenter. Two configurations were considered — v123 with first three recorders and v12345 with all five recorders.

The results of the numerical experiments conducted are in a good agreement with the results obtained from seismic data by other researchers [18]. The main uplift was placed near to the point ( $31^\circ\text{S}, 72.31^\circ\text{W}$ ). As in other studies [19, 21, 22], it has been determined that the tsunami area is located, approximately, 70 km to the NW of the epicenter that coincides with the center of the fault slip [18]. In addition, the extreme values vary from 9 m in the positive and to 6.3 m in the negative displacement and are comparable with those obtained in the studies mentioned above.

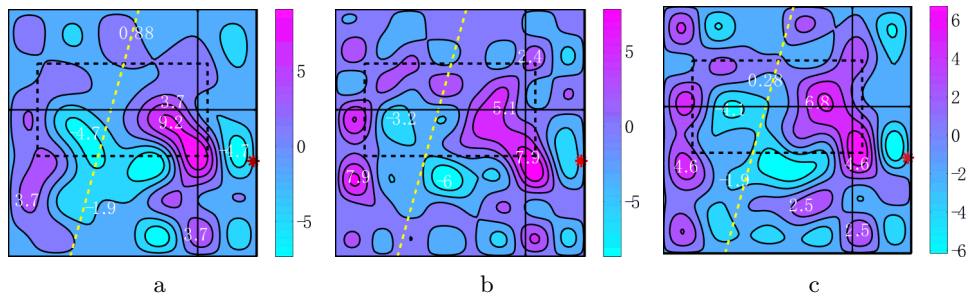


**Figure 4.** The results of recovering the Illapel Chile Tsunami Source in  $\Omega$ : a) v123,  $M = 7$ ,  $N = 7$ ,  $\varphi_{\max} = 12.01$  m,  $\varphi_{\min} = -7.46$  m,  $r = 38$ ; b) v123,  $M = 8$ ,  $N = 8$ ,  $\varphi_{\max} = 10.3$  m,  $\varphi_{\min} = -8.8$  m,  $r = 36$ ; c) v12345,  $M = 8$ ,  $N = 8$ ,  $\varphi_{\max} = 9.01$  m,  $\varphi_{\min} = -6.25$  m,  $r = 36$

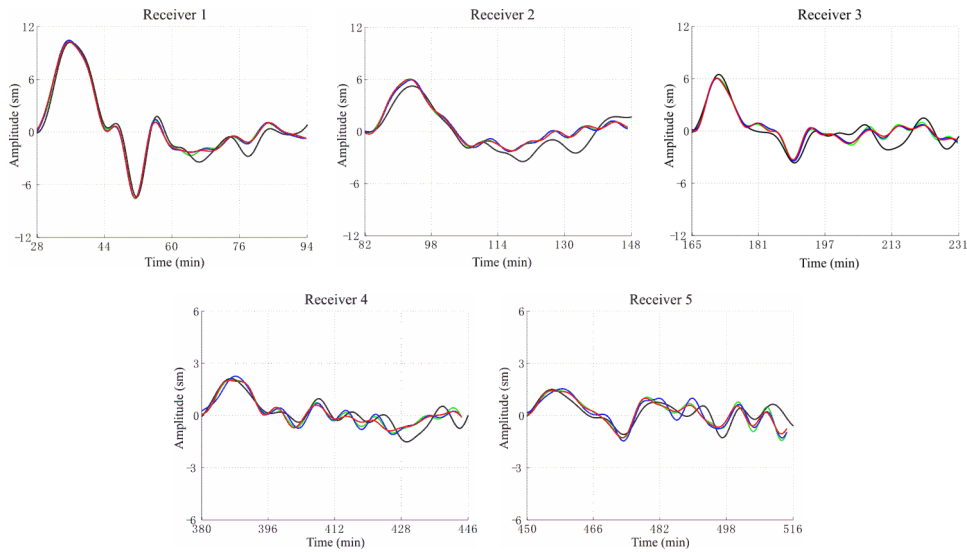


**Figure 5.** A comparison of the observed tsunami waveforms (the black line) with the calculated ones in configurations: v123,  $M = 8$ ,  $N = 8$ ,  $r = 36$  (the blue line); v123,  $M = 7$ ,  $N = 7$ ,  $r = 38$  (the green line); and v12345,  $M = 8$ ,  $N = 8$ ,  $r = 36$  (the red line). The labels on the horizontal axis indicate the time (in minutes) after the earthquake origin time

Moreover, the artifacts to the west direction of the trench did not prevent us from getting a good agreement between the observed and the computed marigrams, which is considered to be a criterion of the quality of the inversion. In addition, the location of the main uplift was reconstructed with a reasonable accuracy.

Figure 5 represents the computed marigrams and the observed ones at each point of observational system. Let us emphasize that using the tsunami waveforms from the recorders 1, 2, 3 only we have also obtained a good matching of the marigrams from the recorders 4 and 5.

#### 4. Conclusion

The numerical simulation of a tsunami source is one of an important component of the assessment and, thus, mitigation of the effects of the tsunami impact.

The problem of retrieving the initial water elevation field based on the inversion of the remote measurements of water-level data is an ill-posed one that imposes severe constraints on the mathematical apparatus employed for solving this problem. The application of  $r$ -solutions is an effective means of regularization of an ill-posed problem which suppresses the instability due to the ill-posedness of the problem and allows one to obtain a reliable result of restoration under the given conditions.

Based on the numerical experiments, it was revealed that the characteristic features of the  $r$ -solution obtained are largely determined by the underlying bathymetry and the observation system. Moreover, using the SVD truncation caused to the appearance the inevitable artifacts in the solution due to using the non-optimal spatial discretization of the unknown function. This paper discusses the way to avoid this obstacle. An observation system can be optimally configured by using this approach.

The method presented provides a good matching in the observed and the calculated tsunami waveforms. In addition, the algorithm provides a possibility to simultaneously restore the tsunami source and calculate tsunami waveforms, even at the points where there are no observational data—there is no need to solve the wave propagation problem once again.

## References

- [1] Satake K. Inversion of tsunami waveforms for the estimation of hereogeneous fault motion of large submarine earthquakes: the 1968 Tokachi-oki and the 1983 Japan sea earthquake // *J. Geoph. Res.* — 1989. — Vol. 94. — P. 5627–5636.
- [2] Piatanesi A., Tinti S., Pagnoni G. Tsunami waveform inversion by numerical finite-elements Green's functions // *Nat. Hazards Earth Syst. Sci.* — 2001. — Vol. 1. — P. 187–194.
- [3] Pires C., Miranda P.M.A. Tsunami waveform inversion by adjoint methods // *J. Geophys. Res.* — 2010. — Vol. 106. — P. 19773–19796.
- [4] Titov V.V., Gonzalez F.I., Bernard E.N., Eble M.C., et al. Real-time tsunami forecasting: Challenges and solutions // *Nat. Hazards.* — 2005. — Vol. 35, No. 1. — P. 45–58.
- [5] Percival D.B., Denbo D.W., Eble M.C., et al. Extraction of tsunami source coefficients via inversion of DART<sub>r</sub> buoy data // *Nat. Hazards.* — 2011. — Vol. 58. — P. 567–590.
- [6] Satake K., Fujii Y., Harada T., Namegaya Y. Time and space distribution of coseismic slip of the 2011 Tohoku earthquake as inferred from tsunami waveform data // *Bull. Seismological Society of America.* — 2013. — Vol. 103, No. 2B. — P. 1473–1492.
- [7] Tinti S., Tonini R. The UBO-TSUF<sub>D</sub> tsunami inundation model: validation and application to a tsunami case study focused on the city of Catania, Italy // *Nat. Hazards and Earth System Sciences.* — 2013. — Vol. 13. — P. 1795–1816.
- [8] Mulia I.E., Asano T. Initial tsunami source estimation by inversion with an intelligent selection of model parameters and time delays // *J. Geoph. Res. Oceans.* — 2016. — Vol. 121. — doi:10.1002/jgrc.21401.
- [9] Romano F., Piatanesi A., Lorito S., et al. Optimal time alignment of tide-gauge tsunami waveforms in nonlinear inversions: Application to the 2015 Illapel (Chile) earthquake // *Geoph. Res. Letters.* — 2016. — Vol. 43. — P. 11226–11235.

- [10] Baba T., Cummins Ph.R., Thio H.K., Tsushima H. Validation and joint inversion of teleseismic waveforms for earthquake source models using deep ocean bottom pressure records: a case study of the 2006 Kuril Megathrust earthquake // *Pure and Appl. Geoph.* — 2009. — Vol. 166, No. 1–2. — P. 55–76.
- [11] Voronina T.A., Tcheverda V.A. Reconstruction of tsunami initial form via level oscillation // *Bull. Novosibirsk Comp. Center. Ser. Math. Model. in Geoph.* — Novosibirsk, 1998. — Iss. 4. — P. 127–136.
- [12] Voronina T.A. Reconstruction of initial tsunami waveforms by a truncated SVD method // *J. Inverse and Ill-posed Problems.* — 2012. — Vol. 19. — P. 615–629.
- [13] Voronin V.V., Voronina T.A., Tcheverda V.A. Inversion method for initial tsunami waveform reconstruction. // *Nat. Hazards Earth Syst. Sci.* — 2015. — Vol. 15. — P. 1251–1263.
- [14] Voronina T.A., Romanenko A.A. The new method of tsunami source reconstruction with r-resolution inversion method // *Pure and Appl. Geoph.* — 2016. — Vol. 173, Iss. 12. — P. 4089–4099.
- [15] Voronina T., Voronin V., Loskutov A. The simulation of the 16 September 2015 Chile (Illapel) tsunami source by the inversion of tsunami waveforms // *Bull. Novosibirsk Comp. Center. Ser. Math. Model. in Geoph.* — Novosibirsk, 2017. — Iss. 20. — p. 57–66.
- [16] Cheverda V.A., Kostin V.I. r-pseudoinverse for compact operator // *Siberian Electronic Mathematical Reports.* — 2010. — Vol. 7. — P. 258–282.
- [17] Voronina T. A., Tcheverda V.A., Voronin V.V. Some properties of the inverse operator for a tsunami source recovery // *Sib. Electronic Mathematical Reports.* — 2014. — Vol. 11. — P. 532–547.
- [18] Satake K., Heidarzaden M. A review of source models of the 2015 Illapel, Chile earthquake and insights from tsunami data // *Pure and Appl. Geoph.* — 2017. — Vol. 174, No. 1. — P. 1–9.
- [19] Heidarzadeh M., Murotani S., Satake K., et al. Source model of the 16 September 2015 Illapel, Chile, Mw 8.4 earthquake based on teleseismic and tsunami data // *Geoph. Res. Letters.* — 2016. — Vol. 43. — P. 643–650.
- [20] Marchuk An.G., Chubarov L.B., Shokin Yu.I. *The Numerical Simulation of the Tsunami Wave.* — Novosibirsk: Nauka, 1983.
- [21] Tilmann F., Zhang Y., Moreno M., et al. The 2015 Illapel earthquake, central Chile: A type case for a characteristic earthquake? // *Geophys. Res. Letters.* — 2016. — Vol. 43. — P. 574–583.
- [22] Li L., Lay T., Cheung K.F., Ye L. Joint modeling of teleseismic and tsunami wave observations to constrain the 16 September 2015 Illapel, Chile, Mw 8.3 earthquake rupture process // *Geophys. Res. Letters.* — 2016. — Vol. 43. — P. 4303–4312.